AFRL-RX-WP-TP-2008-4052

RANDOM HETEROGENEITY SCALES AND PROBABILISTIC DESCRIPTION OF THE LONG-LIFETIME REGIME OF FATIGUE (PREPRINT)

S.K. Jha and James M. Larsen

Universal Technology Corporation

JUNE 2007

AIR FORCE RESEARCH LABORATORY
MATERIALS AND MANUFACTURING DIRECTORATE
WRIGHT-PATTERSON AIR FORCE BASE, OH 45433-7750
AIR FORCE MATERIEL COMMAND
UNITED STATES AIR FORCE

REPORT DOCUMENTATION PAGE

Form Approved
OMB No. 0704-0188

1. REPORT DATE *(DD-MM-YY)*	2. REPORT TYPE	3. DATES COVERED *(From - To)*
June 2007	Technical Paper Preprint	

4. TITLE AND SUBTITLE

RANDOM HETEROGENEITY SCALES AND PROBABILISTIC DESCRIPTION OF THE LONG-LIFETIME REGIME OF FATIGUE (PREPRINT)

5a. CONTRACT NUMBER
F33615-03-D-5801

5b. GRANT NUMBER

5c. PROGRAM ELEMENT NUMBER
62102F

6. AUTHOR(S)

S.K. Jha (Universal Technology Corporation)
James M. Larsen (AFRL/RXLMN)

5d. PROJECT NUMBER
4349

5e. TASK NUMBER
L0

5f. WORK UNIT NUMBER
4349L0VT

7. PERFORMING ORGANIZATION NAME(S) AND ADDRESS(ES)

Universal Technology Corporation
Dayton, OH 45432

Metals Branch, Behavior/Life Prediction Section
(AFRL/RXLMN)
Metals, Ceramics & Nondestructive Evaluation Division
Materials and Manufacturing Directorate
Wright-Patterson Air Force Base, OH 45433-7750
Air Force Materiel Command, United States Air Force

8. PERFORMING ORGANIZATION REPORT NUMBER

9. SPONSORING/MONITORING AGENCY NAME(S) AND ADDRESS(ES)

Air Force Research Laboratory
Materials and Manufacturing Directorate
Wright-Patterson Air Force Base, OH 45433-7750
Air Force Materiel Command
United States Air Force

10. SPONSORING/MONITORING AGENCY ACRONYM(S)
AFRL/RXLMN

11. SPONSORING/MONITORING AGENCY REPORT NUMBER(S)
AFRL-RX-WP-TP-2008-4052

12. DISTRIBUTION/AVAILABILITY STATEMENT

Approved for public release; distribution unlimited.

13. SUPPLEMENTARY NOTES

Conference paper submitted to the Proceedings of the Very High Cycle Fatigue Conference.

 PAO Case Number: AFRL/WS 07-1596, 09 Jul 2007. Paper has color content.

14. ABSTRACT

The long-lifetime fatigue regime is suggested to be a probabilistic realization of sequentially occurring mechanisms. We associate these mechanisms with the development of a ranking of heterogeneity scales in the material, with decreasing probability of occurrence in the order of increasing scale, at any given loading condition. The underlying drivers for these heterogeneity levels are an array of randomly occurring microstructural configurations. With respect to the α+β titanium alloy, Ti-6Al-2Sn-4Zr-6Mo (Ti-6-2-4-6), we identify four microstructural configurations producing different degrees of heterogeneous behavior. At lower stress levels, these configurations present probabilities of failure by a crack-growth-controlled, life-limiting mechanism, and a group of long-lifetime mechanisms. This description of the long-lifetime regime seems to explain the increased incidence of subsurface failures with decreasing stress level, as well as the microstructural neighborhoods involving crack initiation in short and long-lifetime mechanisms and those related to surface and subsurface failures.

15. SUBJECT TERMS

Heterogeneity scales, Microstructural configuration, Probabilistic description, fatigue variability, Ti-6Al-2Sn-4Zr-6Mo, long-lifetime regime, life-limiting mechanism

16. SECURITY CLASSIFICATION OF:			17. LIMITATION OF ABSTRACT:	18. NUMBER OF PAGES	19a. NAME OF RESPONSIBLE PERSON (Monitor)
a. REPORT	b. ABSTRACT	c. THIS PAGE			James M. Larsen
Unclassified	Unclassified	Unclassified	SAR	18	19b. TELEPHONE NUMBER *(Include Area Code)* N/A

Standard Form 298 (Rev. 8-98)
Prescribed by ANSI Std. Z39-18

RANDOM HETEROGENEITY SCALES AND PROBABILISTIC DESCRIPTION OF THE LONG-LIFETIME REGIME OF FATIGUE

S. K. Jha* and J. M. Larsen
US Air Force Research Laboratory, Wright-Patterson Air Force Base, OH 45433, USA
*Universal Technology Corporation, Dayton, OH 45432, USA

Keywords: Heterogeneity scales, Microstructural configuration, Probabilistic description, fatigue variability, Ti-6Al-2Sn-4Zr-6Mo, long-lifetime regime, life-limiting mechanism

Abstract

The long-lifetime fatigue regime is suggested to be a probabilistic realization of sequentially occurring mechanisms. We associate these mechanisms with the development of a ranking of heterogeneity scales in the material, with decreasing probability of occurrence in the order of increasing scale, at any given loading condition. The underlying drivers for these heterogeneity levels are an array of randomly occurring microstructural configurations. With respect to the $\alpha+\beta$ titanium alloy, Ti-6Al-2Sn-4Zr-6Mo (Ti-6-2-4-6), we identify four microstructural configurations producing different degrees of heterogeneous behavior. At lower stress levels, these configurations present probabilities of failure by a crack-growth-controlled, life-limiting mechanism, and a group of long-lifetime mechanisms. This description of the long-lifetime regime seems to explain the increased incidence of subsurface failures with decreasing stress level, as well as the microstructural neighborhoods involving crack initiation in short and long-lifetime mechanisms and those related to surface and subsurface failures.

Introduction

Characterization and understanding of the fatigue behavior in the long-lifetime regime is essential to meet the demand for increased durability of gas turbine engine components [1], as well as, realizing safe operation in the ultra-long cycle regime in many current and emerging applications [2, 3]. In particular, there is a need for a quantitative physics-based analysis of long-lifetime fatigue [4] in order to remove empiricism from life-prediction and management approaches in fracture critical applications [4, 5].

There has been an increased interest in the very high cycle fatigue (VHCF) regime in the recent years [6, 7]. The capability to conduct fatigue tests by ultrasonic excitations has enabled significantly faster experimentation and characterization of behavior beyond 10^7 cycles [6-9]. It is widely accepted that the conventional fatigue limit does not extend to longer lifetimes [10-12]. Often, depending on the material, the long-lifetime regime is accompanied by a step in the stress vs. lifetime (S-N) behavior, which is attributed to a switch in the crack initiation mechanism at lower stress levels [10-12]. In most cases, this change in mechanism has been reported to be associated with a shift from surface to subsurface crack initiation [12-14]. In particular, subsurface crack initiation has been related to non-metallic particles in many studies [10, 12, 13]. This behavior has been explained through existence of multiple thresholds corresponding to initiation of fatigue by each mechanism [11].

The above descriptions of fatigue in the long-lifetime regime seem to relate to the average behavior. Therefore, the understanding of the effect of microstructure and loading variables on fatigue lifetime in this regime has been largely deterministic. A probabilistic description of the long-lifetime behavior appears attractive, given the variable nature of fatigue, but perhaps more so, from a life-prediction perspective. This is owing to an increasing need in the aircraft industry for move towards probabilistic life-prediction, especially, physics-based methodologies [5]. This will remove the large degree of uncertainty in life prediction that might occur in traditional, uncertainty-factor-based design approaches [14]. A probabilistic understanding of fatigue behavior in the long-lifetime regime may therefore, naturally lend itself to emerging life-prediction and life-management practices [5].

Towards a probabilistic description, the competition between mechanisms, in which the final failure in any given loading regime is suggested to occur by the mechanism that produces the shortest lifetime, has been recognized in several studies [11, 12]. Its effect on producing separation of life-limiting and the mean-dominating behavior in the fatigue variability response [15-17] and causing dual S-N curves [18] has been reported recently. Besides the relatively known population of grains and microstructural features, random microstructural neighborhoods and their interaction with the fatigue variability response are relatively unexplored.

Here, we discuss a probabilistic approach to describing the long-lifetime fatigue behavior, and the effect of microstructure and loading variables on the long-lifetime regime of the $\alpha+\beta$ titanium alloy Ti-6-2-4-6. By long-lifetime we mean lifetimes in the range of 10^6 to 10^7 cycles which are not in the very high cycle fatigue (VHCF) regime in the strictest sense, but the same concepts are applicable beyond 10^7 cycles. We show that the long-lifetime fatigue is a result of fatigue variability behavior arising due to sequential probability of occurrence of mechanisms, in order of decreasing level of underlying heterogeneous deformation. Our emphasis has been on identifying the randomly occurring microstructural configurations associated with the heterogeneous response and their relationship to fatigue variability behavior at lower stress levels.

Materials and Experimental Procedure

The materials in this study were two similar microstructures of the $\alpha+\beta$ titanium alloy, Ti-6-2-4-6. These are shown in Fig. 1 (a) and (b) respectively. We designate these as microstructures A and B, as indicated. The microstructures differed slightly in terms of the primary-α structure, in that there was a small increase in the volume fraction of equiaxed-α in microstructure B, along with occasional clusters of a few equiaxed-α grains. The lath-α size in microstructure B was much smaller than in microstructure A, as evident from Fig. 1. In terms of texture, reported in [17], the differences between the two microstructures were more apparent. Particularly, there was greater tendency for the basal and the prismatic poles to be parallel to the loading axis in microstructure B [17].

Some of the experimental procedures in this study have been reported in [15, 17]. The crack initiation facet angles, with respect to the loading axis, were measured using the MeX^{TM} (a trademark of Alicona Imaging GmbH) 3D image analysis program. Stereo-image pairs at relative tilt of 7° were recorded for this purpose using a Lecia S360FE Scanning Electron Microscope. The crack initiation neighborhoods in selected samples were analyzed by sectioning the crack-initiation region using focused ion beam (FIB) machining. A FEI-NOVA^{TM} dual beam FIB system was used for this purpose. A Ga ion beam was employed at the accelerating voltage of 30 kV and the current of 9.3 nA. The FIB sections were made either parallel or perpendicular to the fracture surface. The sectioning step-size was such as to preserve part of the crack initiating

grain. The sectioned planes were then characterized by Electron Back Scattered Diffraction (EBSD) to determine the orientation of the crack initiating grain and the surrounding neighborhood. The inverse pole figure (IPF) plots and maps were constructed using the TSL^{TM} analysis software.

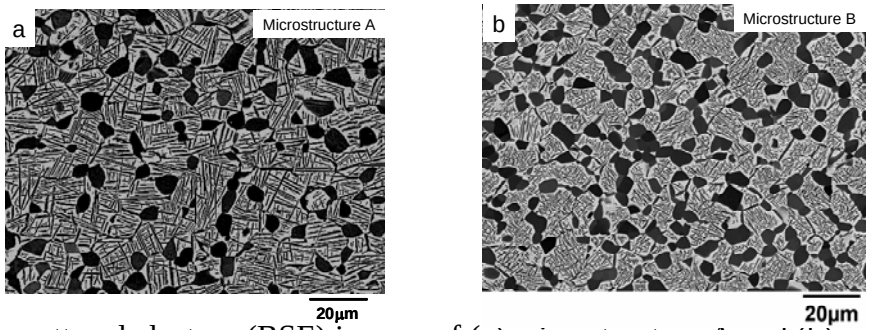

Figure 1. Back-scattered electron (BSE) images of (a) microstructure A and (b) microstructure B of Ti-6-2-4-6.

Probabilistic Description of the Long-Lifetime Regime

The observed long-lifetime fatigue response, producing two-stage S-N curves [11, 12] or failures (in the 10^7 – 10^9 cycles range) by appearance of a different mechanism such as subsurface-inclusion based crack-initiation [7, 10], can be suggested to be a special case of a more general fatigue variability behavior. In particular, we propose that nominally elastic loading produces a ranking of heterogeneity levels in a material, even under the same loading condition. By heterogeneity levels we imply the scale or intensity of localized plastic deformation as caused by randomly existing microstructural neighborhoods. Borrowing the concepts from statistical-physics [19], higher the level of heterogeneity, the smaller is the probability of its occurrence in a sample. It also follows that, for a given crack initiation location (surface or subsurface), the higher the rank of the heterogeneity associated with a mechanism, the shorter is the lifetime.

The above description supposes that deformation can be concentrated in several random microstructural configurations. In a later section, we identify these configurations in Ti-6-2-4-6. The incidence of a given lifetime-range, therefore, may be less dependent on reaching the threshold for a damage accumulation method [11], but controlled by the probability of a microstructural configuration that would produce the necessary heterogeneity level for crack initiation and early propagation. This suggests that, the behavior in the long-lifetime regime corresponds to probabilistic realizations of sequential failure mechanisms, signifying the possibility of both short and long-lifetimes for given microstructure and loading variables.

Long-Lifetime Regime in Ti-6-2-4-6

The fatigue variability behaviors of microstructures A and B of Ti-6-2-4-6 at room temperature are presented in Fig. 2 (a). The deterministic crack growth lifetime limits are superimposed in the figure. The calculations of crack growth bounds were based on the limiting small crack growth curves, shown in Fig. 2(b), and the range in the observed crack initiation sizes [20]. As illustrated in the figure, power-law fits to the small crack data representing the fastest and the slowest crack growth rates were taken as the limiting curves. The crack initiation sizes were measured from the fracture surface and corresponded to the crack initiation facet present at the origin of the crack [20]. The crack growth behaviors of the two microstructures were similar. Therefore, the calculated lifetime bounds can be considered applicable to both cases.

Figure 2 indicates that, in both microstructures, the mean-lifetime behavior (designated as Type II in the figure) diverged from the crack-growth-controlled life-limiting behavior (designated as

Type I) as the stress level was decreased. In [15-17] we describe this behavior by a bimodal probability density. This separation produced up to 500X variability in lifetime at the same stress level. The long-lifetime fatigue regime could, therefore, be a manifestation of decreased probability of occurrence of a microstructural configuration in the specimen surface to enable a purely crack-growth-controlled mechanism. Other mechanisms in the sequence can emerge with varying probabilities, producing much longer lifetimes. However, the latter mechanisms need not be related only to subsurface crack initiation, as evident in Fig. 2(a). According to the suggested probabilistic description, these longer-lifetime mechanisms might be, related to either a smaller heterogeneity scale (therefore, more frequently distributed) at the surface or a larger heterogeneity level (therefore, unlikely to occur at the surface) occurring in the subsurface.

It is also to be noted that the transition from surface to subsurface failure is not abrupt but gradual, with increasing probability of subsurface mechanism occurring with decreasing stress. Szczepanski, et al. [21] show that this trend continues into the 10^7 – 10^9 cycles regime.

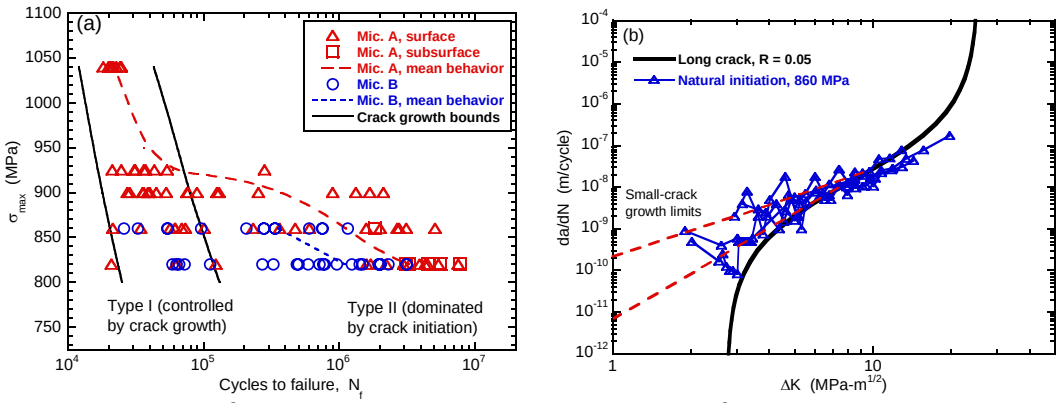

Figure 2. Divergence of the mean-dominating mechanisms from the crack-growth-controlled life-limiting behavior in Ti-6-2-4-6; (a) fatigue variability behavior of microstructures A and B and (b) The small crack growth rate limits used in the calculation.

Different Heterogeneity Scales

Here we attempt to reveal the possible heterogeneous configurations underlying the life-limiting and the long-lifetime (or the mean-dominating) mechanisms. At moderate temperatures, slip in the α phase is considered as the primary deformation mode in α+β titanium alloys [22, 23]. The soft deformation modes are known to be slip in a prismatic <a> system, followed by the basal <a> slip [22]. The deformation in the c-direction of the HCP crystal is accounted by <c+a> slip, which is a significantly harder slip mode [23, 24] when compared to the <a> modes. Although the slip mechanisms in the lamellar α/β colonies are not fully understood, deformation is thought to be accomplished by either prismatic slip parallel to the α/β interface or basal slip across the interface [22, 24]. The later is made possible by the Burger's orientation relationship in the lamellar region: $(0001)_\alpha$ // $\{110\}_\beta$ and $<11\bar{2}0>_\alpha$ // $<111>_\beta$.

Heterogeneity Neighborhoods Associated with Surface Crack Initiation

Typical surface crack initiation regions in Type I (life-limiting) and Type II (mean-lifetime dominating) mechanisms at 860 MPa are shown in Fig. 3(a) and (b) respectively. The crack initiated across an equiaxed-α grain, producing a facet at the crack origin in both mechanisms, as shown. In some cases (especially in Type II failures) more than one facet was seen. Clearly, any differences between the underlying microstructural configurations in the two cases cannot be conclusively ascertained from the fracture surfaces.

A comparison of the surface crack initiation size distribution and the nominal equiaxed-α size distribution revealed that the crack initiation sizes were displaced slightly to the right of the nominal distribution of the equiaxed α [20]. However, the critical facet size was not in the extreme right tail, especially considering that the measured facet area usually represents the largest plane across the grain as opposed to random sections in a nominal measurement [25]. Also, there was no clear trend in the crack initiation size with respect to the lifetime [20]. These results seem to reinforce the important roles of the orientation of the crack initiating grain (besides the size) and the local neighborhood in crack initiation.

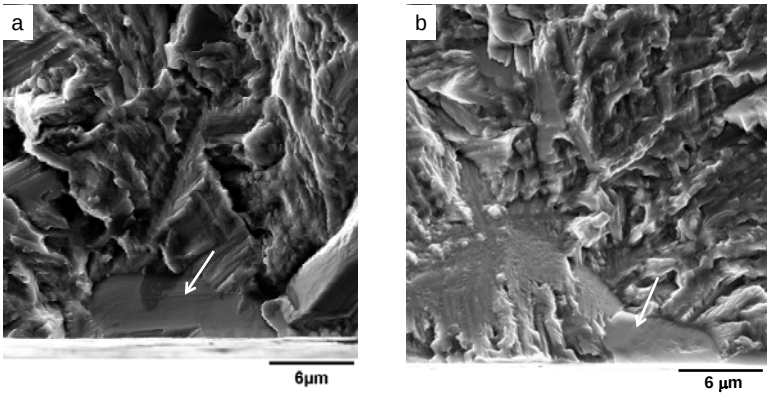

Figure 3. Typical crack initiation morphology in (a) a Type I mechanism tested at 860 MPa that failed in 72,977 cycles and (b) a Type II mechanism tested at 860 MPa and having the lifetime of 2,755,245 cycles.

In Fig. 4, the angle of the crack initiation facet normal with the loading axis (indicated as θ in the figure) is plotted with respect to lifetime for the two microstructures of Ti-6-2-4-6. The data points correspond to the applied stress levels of 860 and 820 MPa. As shown, irrespective of lifetime, surface crack initiation facets in microstructure A were at an angle of about 35 - 45° from the loading axis. The spread in the angles was slightly larger in microstructure B. Figure 4 indicates that, in both Type I and Type II surface crack initiation, these facets were oriented for close to maximum shear, i.e., slip deformation.

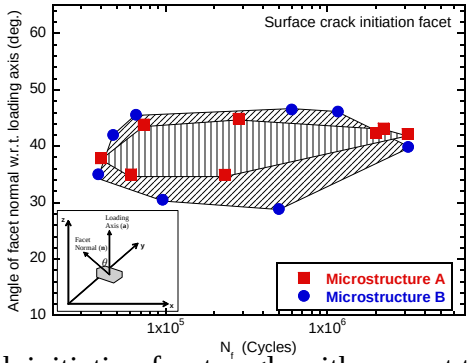

Figure 4. Crack initiation facet angle with respect to the loading axis.

Examples of FIB sections of the crack initiation region in a Type I and a Type II mechanism are shown in Figs. 5 and 6 respectively. The crack origin in a sample tested at 860 MPa that failed in 61,162 cycles (Type I) is shown in Fig. 5(a). The crack initiation facet is indicated in the figure. The facet angle with respect to the loading axis was 35.02°. In this case, the FIB surface was parallel to the fracture surface. The Inverse Pole Figure (IPF) map (in the loading direction) from the FIB sectioned plane is shown in Fig. 5(b). The crack initiating equiaxed-α grain is identified in the figures. The IPF map indicates that the crack initiating grain had a close to basal orientation with respect to the loading axis. This would mean that, in Type I failures, the crack initiation facet may be formed by a <c+a> hard slip mechanism.

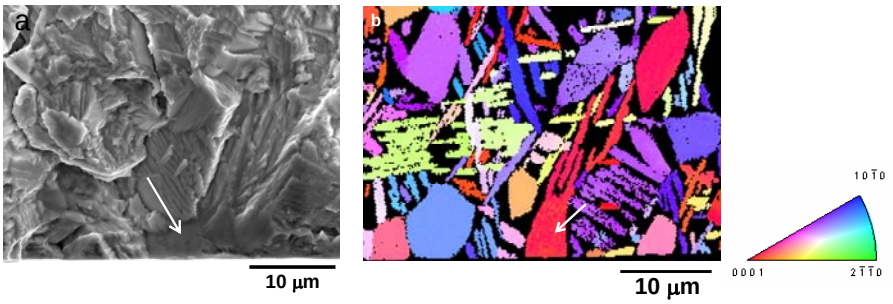

Figure 5. FIB sectioning and OIM analysis of crack initiation region in a Type I failure; (a) the crack initiation region and (b) IPF map, in the loading direction, of the FIB plane (machined parallel to the fracture surface).

The crack initiation region in a Type II failure at 860 MPa is shown in Fig. 6(a). The lifetime in this case was 1,996,709 cycles. The crack initiation facet is indicated. The facet angle with respect to the loading axis was 42.33°. In this sample, the FIB section was made perpendicular to the fracture surface, at about 2 μm from the sample edge, as indicated by the dashed line. Only a part of the crack initiating α grain was sectioned through, as illustrated. The partially sectioned crack initiating α grain is indicated by the arrow. The IPF map, in the direction of the loading axis, is shown in Fig. 6(b). Clearly, in this case, the crack initiating α grain does not have a basal orientation with reference to the loading axis, unlike the Type I mechanism.

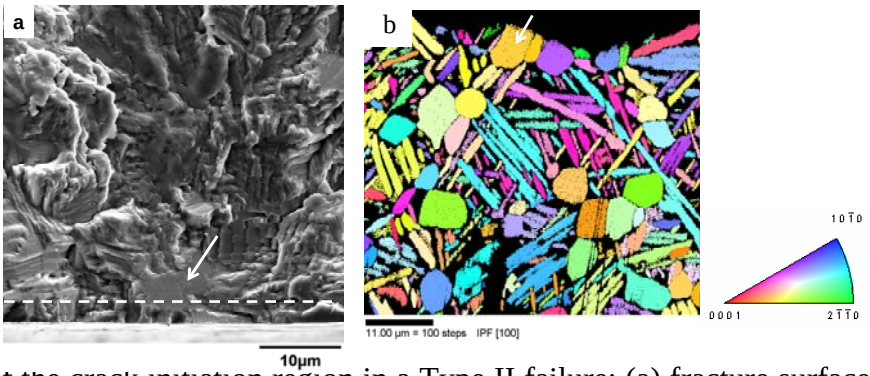

Figure 6. Analysis of the crack initiation region in a Type II failure; (a) fracture surface showing the crack initiation region, (b) IPF map of the FIB plane in the loading direction.

The orientation of crack initiating α grain in three Type I, and a Type II failure, measured by the procedure described above, are plotted in stereographic triangles in Fig. 7. The Schmid Factor (SF) contour lines [24] are superimposed in these figures. The SF contours for prismatic <a>, basal <a>, 1st order pyramidal <c+a>, and 2nd order pyramidal <c+a> are shown in Figs. 7 (a), (b), (c), and (d) respectively. Firstly, as expected from the IPF maps, the Type I points (indicated by the circular symbol) plot close to the basal pole. Furthermore, Figs. 7(a) and (b) indicate that the crack initiating α-grains, in the Type I mechanism, were not in the high SF regions for either prismatic <a> or basal <a> slip. On the other hand, Figs. 7(c) and (d) indicate that these points were very close to maximum SF for either 1st order or 2nd order pyramidal <c+a> slip (both being significantly harder slip modes compared to the prismatic <a> and the basal <a> slip). The crack initiating grain in the Type II mechanism (indicated by the square symbol in Fig. 7) was oriented close to maximum SF for the soft, basal <a>, slip (Fig. 7(b)).

From the argument of different heterogeneity levels, it is known that an α grain oriented for hard slip, surrounded by soft grains or colonies presents a location of significant stress concentration [22, 23]. This kind of microstructural configuration can be considered to be a higher ranked heterogeneity scale than a favorably oriented primary-α, as in the Type II mechanism.

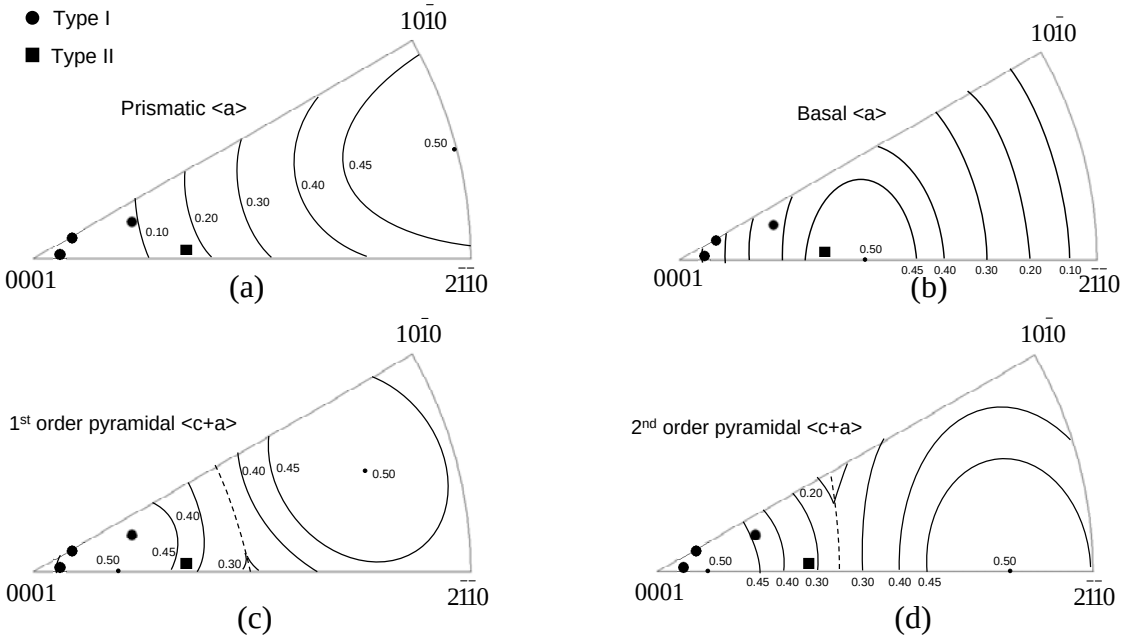

Figure 7. Deformation mechanisms of crack initiating primary-α grain in Type I and Type II mechanisms with the help of SF contour maps for (a) prismatic <a> slip, (b) basal <a> slip, (c) 1st order pyramidal <c+a> slip, and (d) 2nd order pyramidal <c+a> slip.

The poles representing the α lath (in lamellar colonies) and the primary-α grains, neighboring the crack initiating α grain in the two mechanisms, were also plotted in stereographic triangles. The purpose was to determine the possible deformation characteristics of the neighborhood in relation to the crack initiating grain that would highlight further differences between the two mechanisms. This is shown in Figs. 8 and 9 for Type I and Type II mechanisms respectively. The contour lines representing SF for prism <a> and basal <a> slip are superimposed in Fig. 8 (a) and (b) respectively. In Fig 8, neighboring grains from the three Type I samples, as in Fig. 6, are plotted. The lath-α is represented by the circular symbol and the equiaxed-α grain is shown by the square symbol. In the Type I mechanism (Fig. 8), almost all neighboring grains from the three samples were away from the hard <c+a> slip mode (i.e., away from the basal orientation). It is also striking that none of the neighboring poles, in the Type I mechanism, plot near the $(2\bar{1}\bar{1}0)$ plane (Fig. 8).

As stated before, slip in lamellar colonies is said to occur by prismatic <a> mode (in α-lath) along the interface, or basal <a> slip across the colony due to alignment of $(0001)_\alpha$ and $(110)_\beta$ slip planes per the Burger's relationship [22]. Accordingly, only one out of the three possible prismatic <a> slip systems can be active in the lamellar phase [22]. Therefore, high SF for prismatic <a> slip is a necessary but not the sufficient condition for slip. However, all of the three basal <a> systems can be active, provided the α-lath is oriented for the basal slip [22]. Figure 8(b) indicates that a majority of the neighboring lath-α, in the Type I mechanism, plot between SF of about 0.35 and 0.5 for basal <a> slip, implying that these neighboring colonies were oriented for easy deformation mode. The remainder of α laths (total of 7) shows high (between about 0.4 and 0.5) SF for prismatic <a> slip, as indicated by Fig. 8(a). However, in order to confirm that these neighboring colonies were "soft", it needs to be ascertained if the prismatic planes in these laths are parallel to the α/β interface. Figures 8 (a) and (b) also indicate that most of the neighboring primary-α (square symbols) grains, in the Type I mechanism, were oriented for either prismatic <a> or basal <a> slip. Although it remains to be verified if the prismatic <a> systems in laths with high SF for that slip are parallel to the α/β interface, it appears that the microstructural neighborhood in Type I mechanism consists of a hard primary-α

grain surrounded by soft lamellar colonies and primary-α. This is also consistent with suggestions in other studies [22, 23] that this kind of configuration presents enhanced stress concentration at the basal-oriented primary-α due to strain incompatibility with the easily deforming neighborhood. Crack initiation in the Type I mechanism can be suggested to occur by cracking across a pyramidal plane in a close to basal-oriented primary-α that is surrounded by "easy-slip" colonies and equiaxed-α grains.

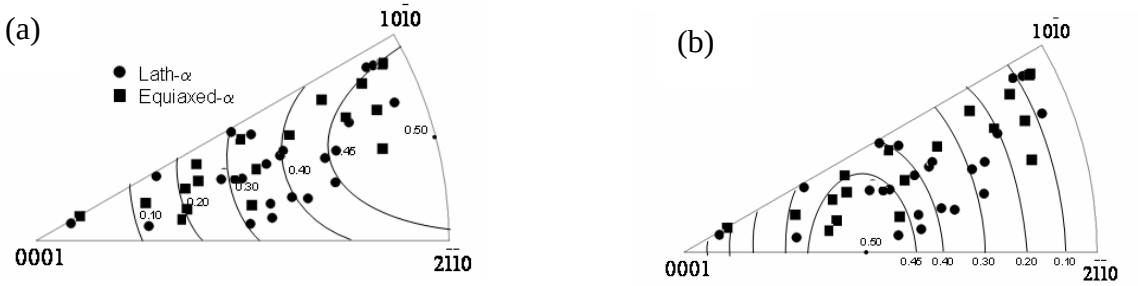

Figure 8. Possible slip behavior of lath and equiaxed α neighboring the crack initiating grain in Type I failures; (a) prismatic <a> contour map and (b) basal <a> contour map.

The poles of lath-α and primary-α neighboring the crack initiating grain in the Type II mechanism are plotted in Fig. 9. The closed circles represent the lath-α and the closed squares indicate the equiaxed-α grains. In this case, again, almost all neighboring α laths and grains are away from the hard, basal orientation. There is an equal mix of lath-α with high SF for basal <a> and those with high SF for prismatic <a> slip. We haven't determined if the ones oriented for prismatic <a> slip satisfy the condition for easy deformation of the colony. It is, therefore, hard to draw conclusions towards the extent to which these neighboring colonies and grains played a role in crack initiation in the Type II mechanism. It seems clear, however, that in the Type II surface initiated failures, crack initiated by slip accumulation in a (or a few) favorably oriented (for basal <a> slip) α grain(s). This is similar to the conventional slip band cracking mechanism that is associated with the creation of surface steps [11].

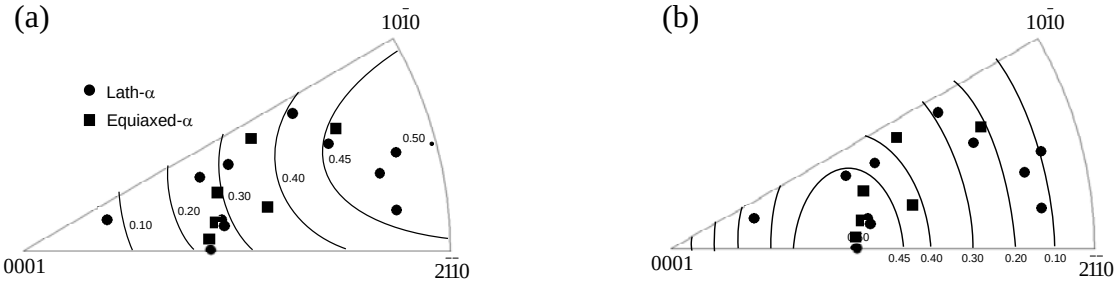

Figure 9. Possible slip mechanisms of lath and equiaxed-α neighboring the crack initiating grain in a Type II failure; (a) prismatic <a> SF contours and (b) basal <a> SF contours.

Heterogeneity Scales Associated with Subsurface Crack Initiation

As shown in Fig. 2(a), in addition to surface crack initiation, the mean-dominating (Type II) distribution also comprised of the subsurface initiated mechanism. Two different kinds of subsurface crack initiation characteristics were observed. Examples of these are presented in Figs. 10 and 11. In the first (Fig. 10(a)), the crack initiation facet appeared to correspond to a cluster of equiaxed α and lamellar α/β colonies producing a continuous, relatively large crack initiation facet. The angle of this facet with respect to the loading axis was measured at multiple locations (labeled in Fig. 10(a)). The measurements are shown in Fig. 10(b) and indicate that the angles were very similar at each of the locations, confirming that the crack initiation facet is continuous. The average angle with respect to the loading axis was about 44° suggesting that the facet was formed due to continuous slip in a microstructural cluster that included equiaxed-α and

lamellar colonies. We have not yet analyzed the crystallographic direction of the facet constituents with respect to the loading axis. However, it can be suggested that the slip planes of the constituent phases in the facet were aligned.

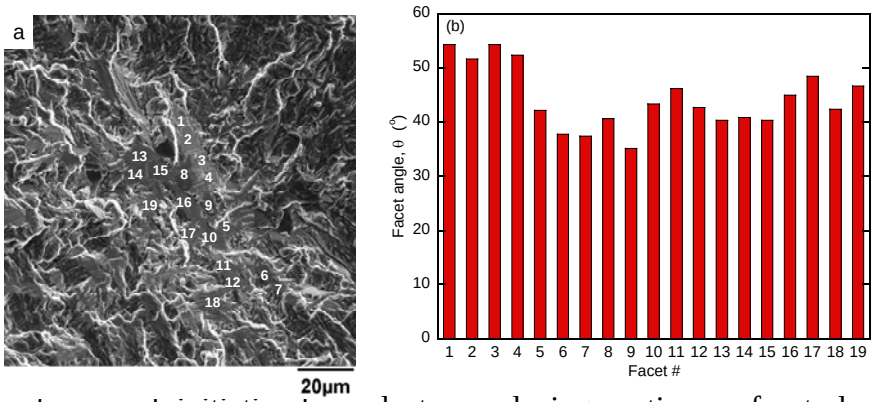

Figure 10. Subsurface crack initiation by a cluster producing continuous facet plane (σ_{max} = 820 MPa, N_f = 3,088,204); (a) the crack origin and (b) facet angles at the locations labeled in (a).

The second subsurface crack initiation characteristic observed in Ti-6-2-4-6 is shown in Fig. 11(a). In this case, we observe a cluster of equiaxed-α grain facets, over a relatively large region, at the crack origin. Szczepanski, et al [22] have also identified this as the predominant subsurface crack initiation mechanism at ultrasonic loading frequencies. The angles of these facets, with respect to the loading axis, are shown in Fig. 11(b). Once again, all facets belonging to the cluster were oriented similarly and the angles were in the range of about 31-53°, i.e., close to maximum shear. Szczepanski and coworkers [22] have determined that most of the facet-forming equiaxed-α grains were close to basal <a> slip orientation. The lifetimes in this subsurface crack initiation configuration were generally longer than the one shown in Fig. 10.

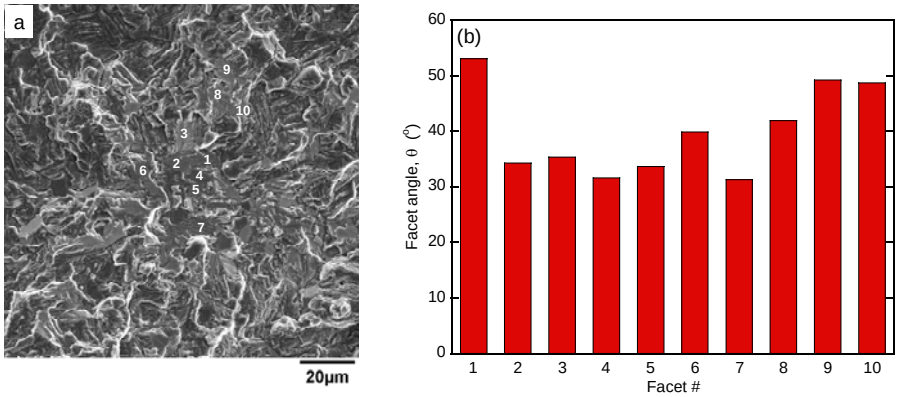

Figure 11. Subsurface crack initiation by a primary-α cluster (σ_{max} = 820 MPa, N_f = 4,487,636); (a) the crack origin and (b) facet angles.

Ranking of Heterogeneity Scales

Based on the above discussion, in Ti-6-2-4-6, at least 4 heterogeneity levels can be identified. The underlying microstructural configurations are schematically illustrated in Fig. 12. In the order of decreasing intensity of deformation accumulation, these are: (i) Cluster of equiaxed-α and lamellar α/β colonies with aligned slip planes and oriented for close to maximum shear, (ii) Cluster of equiaxed-α grains, each similarly oriented for basal <a> slip, (iii) A hard equiaxed-α (oriented for pyramidal <c+a> slip) surrounded by soft lamellar colonies and primary-α, and (iv) A (or a few) favorably oriented (for basal <a>) equiaxed-α grain(s). It follows from our earlier argument that, the probability of occurrence of these configurations will decrease in the order of increasing scale of heterogeneity.

Recognizing the difference between the free surface and the subsurface location with respect to fatigue, the four heterogeneous configurations in Fig. 12 can be arranged into at least 8 possible failure mechanisms. However, due to decreasing probability of occurrence with increasing heterogeneity level, it seems that only 4 mechanisms (2 surface-initiated and 2 subsurface) were observed in the given number of tests. The ranking of heterogeneity levels and the associated probabilities seems to explain the observation that the two surface-initiated mechanisms corresponded to two relatively smaller scale configurations (Fig. 12).

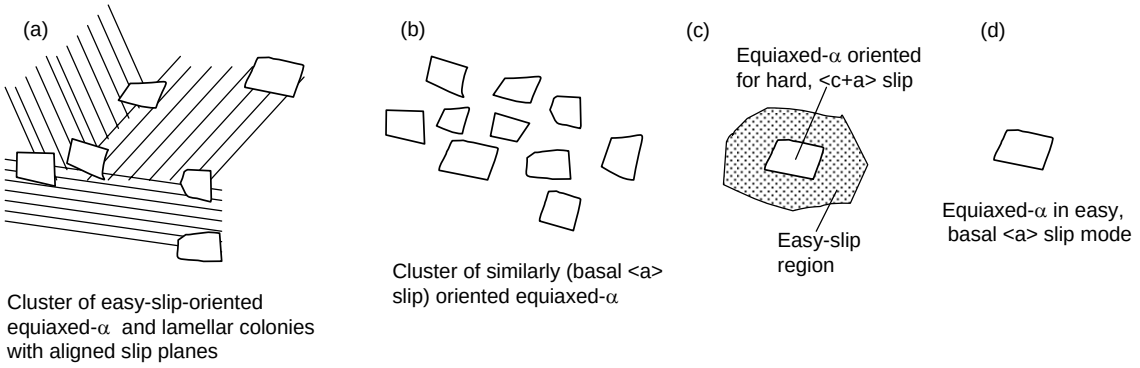

Figure 12. Illustration of randomly occurring microstructural configurations in Ti-6-2-4-6 producing a ranking of heterogeneity scales.

The ranking of heterogeneity scales and their interaction with surface and the subsurface location can be suggested to produce the following sequence of mechanisms in this study: (i) surface initiated failure from a hard primary-α (Fig. 12(c)), (ii) surface crack initiation in a (or a few) favorably oriented primary-α (Fig. 12(d)), (iii) subsurface crack initiation from a cluster of equiaxed-α and lamellar colonies (Fig. 12(a)), and (iv) subsurface crack initiation from an equiaxed-α cluster (Fig. 12(d)). It is to be noted that, the probabilities of occurrence of any given level of heterogeneous deformation will decrease with decreasing stress level, implying a continued shift towards failures by higher ranked random microstructural configurations. This may explain the increased incidence of subsurface initiated failures with decreasing stress level. However, the occurrence of the surface initiated mechanism in the very long-lifetime regimes cannot be ruled out. In those regimes, surface failures can be realized by higher ranked heterogeneity scales, for example, by a cluster of similarly oriented primary-α. Although the probability of occurrence of such mechanism at the surface will decrease for a larger scale of associated microstructural configuration, this ought to be accounted for from a life-prediction perspective. The probabilistic description of the long-lifetime regime discussed here also explains the observations that the long-lifetimes occur either by surface failures from a small heterogeneity scale (as in a favorably oriented primary-α) or by subsurface failures from a large heterogeneity scale (as in clusters with aligned slip planes). Finally, it can be emphasized that the present probabilistic description of long-lifetime regime provides a physical-basis for fatigue variability by accounting for randomly occurring microstructural scales. As such, it may be very advantageous in reducing the uncertainty in lifetime prediction [16, 17].

Conclusions

The following primary conclusions can be drawn from this study:

(i) The long-lifetime regime in Ti-6-2-4-6 could be described as a probabilistic realization of surface-crack-growth controlled mechanism or mean-lifetime dominating mechanisms.

(ii) Four randomly occurring microstructural configurations were identified, which were related to different heterogeneity scales at the same loading condition.

(iii) The surface short-lifetime mechanism occurred by cracking along, or near, pyramidal planes in an equiaxed-α oriented for hard, <c+a> slip.
(iv) The surface long-lifetime mechanism occurred by slip in a favorably oriented (for basal <a> slip) primary-α grain.
(v) The subsurface long-lifetime mechanisms occurred in the region of larger microstructural configurations than the surface failures.
(vi) The probabilistic description of the long-lifetime regime appeared to explain the increasing incidence of subsurface mechanism with decreasing stress level, as well as the heterogeneity scales associated with surface and subsurface failures.

Acknowledgements

This work was performed at the Air Force Research Laboratory, Materials and Manufacturing Directorate, Wright-Patterson Air Force Base, OH. The financial support of the Air Force Office of Scientific Research (AFOSR) through the AFOSR task no. 92ML02COR with Dr. Victor Giurgiutiu as the program manager is gratefully acknowledged. We are also grateful for the partial financial support of the Defense Advanced Research Project Agency (DARPA) under DARPA orders M978, Q588, P699, and S271 with Dr. Leo Christodoulou as the program manager. We acknowledge Mr. Phil Buskohl and Ms. Lindsey Selegue for their assistance with the replication-based small-crack growth experiments. We also wish to acknowledge Dr. Mike Caton, Dr. Andy Rosenberger, and Dr. Reji John for very helpful discussions.

References

1. J. C. Williams and E. A. Starke, Jr., "Progress in Structural Materials for Aerospace Systems," *Acta Materialia*, 51 (2003), 5775-5799.
2. Claude Bathais and Paul C. Paris, *Gigacycle Fatigue in Mechanical Practice* (CRC Press, 2004).
3. C. L. Muhlstein, E. A. Stach, and R. O. Ritchie, "Mechanism of Fatigue in Micron-Scale Films of Polycrystalline Silicon for Microelectromechanical Systems," *Applied Physics Letters*, 80 (2002), 1532-1534.
4. B. A. Cowles, "High Cycle Fatigue in Aircraft Gas Turbines – An Industry Perspective," *International Journal of Fracture*, 80 (1996), 147-163.
5. L. Christodoulou and J. M. Larsen, "Using Materials Prognosis to Maximize the Utilization Potential of Complex Mechanical Systems," *JOM*, (2004), 15-19.
6. S. Stanzl-Tschegg and H. Mayer, Eds., *Proceedings of the International Conference on Fatigue in the Very High Cycle Regime*, Institute of Meteorology and Physics, Vienna, Austria, 2001.
7. Y. Murakami, M. Takada, and T. Toriyama, "Super-long life tension-compression fatigue properties of quenched and tempered 0.46% carbon steel," *International Journal of Fatigue*, 16 (1998), 661-667.
8. H. Mayer, M. Papakyriacou, R. Pippan, and S. Stanzl-Tschegg, "Influence of Loading Frequency on the High Cycle Fatigue Properties of AlZnMgCu1.5Al Alloy," *Materials Science & Engineering A*, 314A (2001), 48-54.
9. A. Shyam, C. J. Torbet, S. K. Jha, J. M. Larsen, M. J. Caton, C. J. Szczepanski, T. M. Pollock, and J. W. Jones, *Superalloys-2004*, Proceedings of the 10th International Conference on Superalloys, T. M. Pollock, et al., Eds., 2004, 259-268.
10. K. Tanaka and Y. Akiniwa, "Fatigue Crack Propagation behavior Derived from S-N Data in Very High Cycle Fatigue," *Fatigue and Fracture of Engineering Materials and Structures*, 25 (2002), 775-784.

11. H. Mughrabi, "On 'Multi-Stage' Fatigue Life Diagrams and the Relevant Life-Controlling Mechanisms in Ultrahigh-Cycle Fatigue," *Fatigue and Fracture of Engineering Materials and Structures*, 25 (2002), 755-764.
12. S. K. Jha and K. S. Ravi Chandran, "An Unusual Fatigue Phenomenon: Duality of the S-N Fatigue Curve in the β-Titanium Alloy Ti-10V-2Fe-3Al," *Scripta Materialia*, 48 (2003), 1207-1212.
13. Q. Y. Wang, C. Bathais, N. Kawagoishi, and Q. Chen, "Effect of Inclusion on Subsurface Crack Initiation and Gigacycle Fatigue Strength," *International Journal of Fatigue*, 24 (2002), 1269-1274.
14. J. W. Lincoln, "Risk Assessment of an Aging Military Aircraft," *Journal of Aircraft*, 22 (1985), 687-691.
15. S. K. Jha, J. M. Larsen, A. H. Rosenberger, and G. A. Hartman, "Dual Fatigue Failure Modes and Consequences on Probabilistic Life Prediction," *Scripta Materialia*, 48 (2003), 1637-1642.
16. S. K. Jha, J. M. Larsen, and A. H. Rosenberger, "The Role of Competing Mechanisms in the Fatigue Life Variability of a Nearly-Fully Lamellar γ-TiAl based Alloy," *Acta Materialia*, 53 (2005), 1293-1304.
17. S. K. Jha, M. J. Caton, and J. M. Larsen, "A New Paradigm of Fatigue Variability Behavior and Implications for Life Prediction," *Materials Science and Engineering A*, article in press, DOI: 10.1016/j.msea.2006.10.171 (2007).
18. K. S. Ravi Chandran and S. K. Jha, "Duality of the S-N Fatigue Curve Caused by Competing Failure Modes in a Titanium Alloy and the Role of Poisson Defect Statistics," *Acta Materialia*, 53 (2005), 1867-1881.
19. K. H. Hoffmann and M. Schreiber, Eds., *Computational Statistical Physics*, Springer, 2001.
20. S. K. Jha, J. M. Larsen, and A. H. Rosenberger, "Microstructure and Temperature Effects on the Fatigue Variability Behavior of an α+β Titanium Alloy and Implications for Life Prediction," *Fatigue-2006*, Proceedings of the 9th International Fatigue Congress, Atlanta, GA, 2006.
21. C. J. Szczepanski, S. K. Jha, J. M. Larsen, and J. W. Jones, "The Role of Microstructure on Fatigue Lifetime Variability," *VHCF-4*, Proceedings of the 4th Very High Cycle Fatigue Conference, Ann Arbor, MI, 2007.
22. J. R. Mayeur, "*Three Dimensional Modeling of Titanium-Aluminum Alloys with Application to Attachment Fatigue*," Masters Thesis, Mechanical Engineering, Georgia Institute of Technology, 2004.
23. V. Hasija, S. Ghosh, M. J. Mills, and D. Joseph, "Deformation and Creep Modeling in Ti-6Al Alloys," *Acta Materialia*, 51 (2003), 4533-4549.
24. H. Tan, H. Gu, C. Laird, and N. D. H. Munroe, "Cyclic Deformation Behavior of High Purity Titanium Single Crystals: Part I. Orientation Dependence of Stress–Strain Response," *Metallurgical and Materials Transactions A*, 29A (1998), 507-512.
25. J. E. Spowart, B. Maruyama, and D. B. Miracle, *Materials Science and Engineering A*, "Multi-scale Characterization of Spatially Heterogeneous Systems: Implications for Discontinuously Reinforced Metal-Matrix Composite Microstructures, A307 (2001), 51-66.